AD-A266 184

TATION PAGE

Form Approved
OMB No. 0704-0188

1. AGENCY USE ONLY (Leave blank)	2. REPORT DATE	3. REPORT TYPE AND DATES COVERED
	31 MAY 93	Final 1 JUN 90 - 31 MAY 93

4. TITLE AND SUBTITLE
Large Signal Characterization and Modeling of Heterojunction Bipolar Transistors

5. FUNDING NUMBERS
G AFOSR-90-0302
PR 2305/R1

6. AUTHOR(S)
D.S. Whitefield, C.J. Wei, J.C.M. Hwang

7. PERFORMING ORGANIZATION NAME(S) AND ADDRESS(ES)
Lehigh University
Department of Electrical Engineering and Computer Science,
Packard Laboratory, 19 Memorial Drive West
Bethlehem, PA 18015-3084

8. PERFORMING ORGANIZATION REPORT NUMBER
AFOSR-TR-93-0438

9. SPONSORING/MONITORING AGENCY NAME(S) AND ADDRESS(ES)
AFOSR/NE
Building 410
Bolling AFB DC 20332-6448

10. SPONSORING/MONITORING AGENCY REPORT NUMBER
2305/R1

11. SUPPLEMENTARY NOTES

12a. DISTRIBUTION/AVAILABILITY STATEMENT
unlimited

13. ABSTRACT (Maximum 200 words)

The high power operation of the heterojunction bipolar transistor (HBT) has been analyzed by experimentally determining the junction temperature and separating temperature effects from other high power effects. In addition, an HBT large signal model has been developed that is valid for the linear, saturation , and cutoff regions, with low frequency temperature effects included. This model has been implemented in a commercial harmonic balance simulator, LIBRA from EEsof, making it particularly suitable for the design and simulation of HBT microwave power integrated circuits. In addition, an analysis of the most temperature-sensitive microwave elements for the HBT has been performed using measured s-parameter data at five elevated temperatures from 23°C to 226°C. The element values were compared to a physical model showing excellent agreement in magnitude and direction of change with temperature and bias. The transistor cutoff frequencies were also measured and calculated, showing a monotonic decrease with temperature of approximately 50% over the 200°C range.

14. SUBJECT TERMS	15. NUMBER OF PAGES
Heterojunction Bipolar Transistor Large Signal Modeling; Thermal Effects	29
	16. PRICE CODE

17. SECURITY CLASSIFICATION OF REPORT	18. SECURITY CLASSIFICATION OF THIS PAGE	19. SECURITY CLASSIFICATION OF ABSTRACT	20. LIMITATION OF ABSTRACT
UNCLASSIFIED	UNCLASSIFIED	UNCLASSIFIED	SAR

Contents

1. Objectives

The main objective of this three year research effort was to investigate the large-signal characteristics of the heterojunction bipolar transistor (HBT) in order to apply the knowledge gained to improve both HBT device and circuit design.

Through innovative approaches for large-signal characterization and modelling, the following specific objectives were accomplished:

- Effective parameter extraction from dc and RF measurements to provide feedback to HBT device design.
- Accurate large-signal measurements in the frequency domain, taking into account the effects of harmonic magnitudes and phases.
- Non-linear equivalent circuit modeling for efficient de-embedding from dc and RF characteristics.
- Characterization of thermal effects relating to high-power and large-signal operation.

2. Progress

The objectives of this project have been met, resulting in accurate characterization and modeling of dc, pulsed, and microwave large signal behavior as well as the related thermal effects.

Many types of measurements have been set up and performed to fully characterize the heterojunction bipolar transistor (HBT). The measurements include dc, pulsed, RF, small signal, power, harmonic and elevated temperature tests as will be described in the following. Most measurements were performed on-wafer which eliminates substrate thinning, dicing and packaging and allows for rapid characterization. The devices characterized were GaAs/AlGaAs HBTs fabricated by the Air Force Wright Laboratory with either three 1μ x 8μ emitters, or a single 1μ x 8μ emitter. The Al concentration at the base emitter junction was graded from 0.3 to 0.0. The substrate thickness was 625μm.

The high power operation of the HBT has been analyzed by experimentally determining the junction temperature and separating temperature effects from other high power effects.

An HBT large signal model has been developed that is valid for the linear, saturation, and cutoff regions, with temperature effects included. This model has been implemented in a commercial harmonic balance simulator, LIBRA from EEsof, making it particularly suitable for the design and simulation of HBT microwave power integrated circuits.

In addition, elevated temperature microwave measurements and modeling have been performed up to 226°C.

2.1 dc and RF Characterization

The equipment used for dc characterization and device biasing includes an HP4142 Semiconductor Parametric Analyzer equipped with three source and monitoring units of either voltages or currents. For high frequency measurements the equipment used included an HP8510-B, a 40 GHz network analyzer with a two port S-parameter test-set, and a HP70206A 26 GHz spectrum analyzer. Calibration of the test equipment was performed on-wafer using a Tektronix calibration substrate.

The dc characterization performed on the HBTs included common emitter I-V, collector and base current vs base voltage, floating collector, and breakdown measurements. All of these result in parameters used as starting points for determining RF equivalent circuit parameters.

RF small-signal S-parameter measurements were performed at bias points over the entire active region of the HBTs. These sets of data were used to extract model element values using optimization techniques. The bias-dependent element values where then used in the large signal model. Power and harmonic measurements were performed up to 2 W/mm and used to confirm large signal model predictions.

2.2 Low Frequency Elevated Temperature Measurements

For on-wafer measurements even at moderate power levels, un-packaged and un-thinned HBTs exhibit significant thermal effects. For the HBT, the undesirable thermal effects result in a reduction of gain and an significant change in base-emitter diode characteristics.

To analyze the thermal effects, dc measurements were performed on an HBT inside an oven. Full sets of I-V characteristics were measured from 23°C to 200°C. The base-emitter voltage (V_{be}) was monitored as a function of temperature and collector voltage for different base currents. V_{be} was found to be a very accurate indication of the actual junction temperature and is shown in Figure 1 to be linear to within 0.4%. For this set of data the collector voltage was chosen to be in the forward active region, but kept at a minimum to limit the power dissipation. V_{be} was, however, found to be independent of collector voltage at low power densities where self heating is negligible.

For room temperature I-V measurements the base-emitter voltage is monitored and used to calculate the junction temperature. For this device, having a 625 μm substrate, all points in the forward active region are consistent with a thermal resistance of 2.9 C/mW to within 10% as seen in Figure 2. This thermal resistance is from the base-emitter junction to the ambient, and is used to obtain the temperature contours on a plot of I-V characteristics as seen in Figure 3.

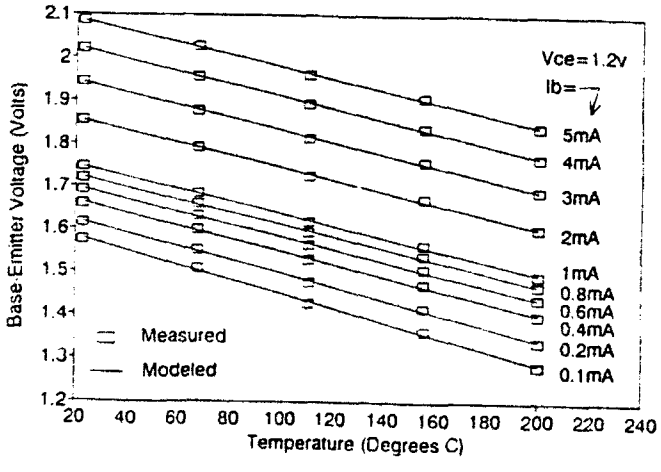

Figure 1. The dependence of base-emitter voltage on ambient temperature.

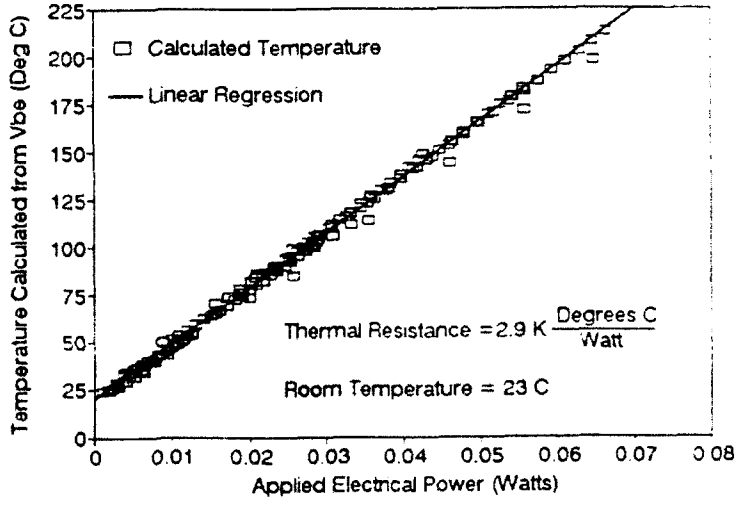

Figure 2. Junction Temperature Calculated from the base-emitter voltage.

The gain degradation as the junction temperature increases is shown in Figure 4. The degradation is essentially linear at -0.0038 /C. The data in this figure includes the forward active region up to where the collector current increases through breakdown. Extrapolating these lines back to room temperature, the Kirk effect can be seen to reduce gain at high base currents (I_b) independent of the temperature effect. Notice that the maximum gain occurs at I_b = 4 mA, and the Kirk effect causes a reduction of gain at I_b = 5 mA.

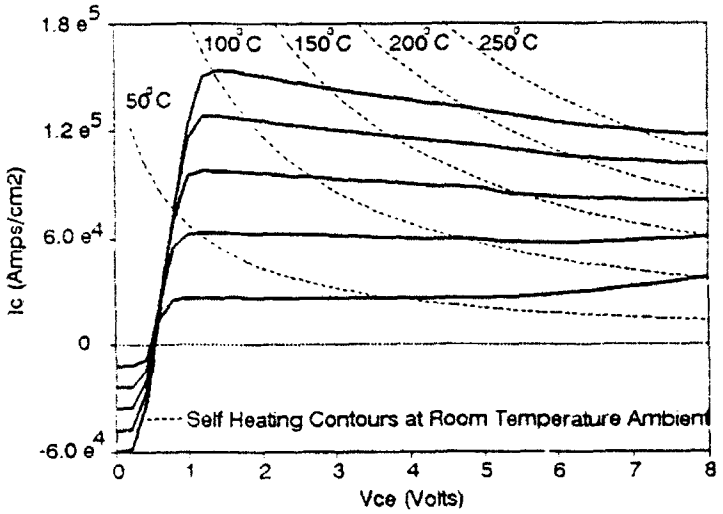

Figure 3. HBT self-heating temperature contours.

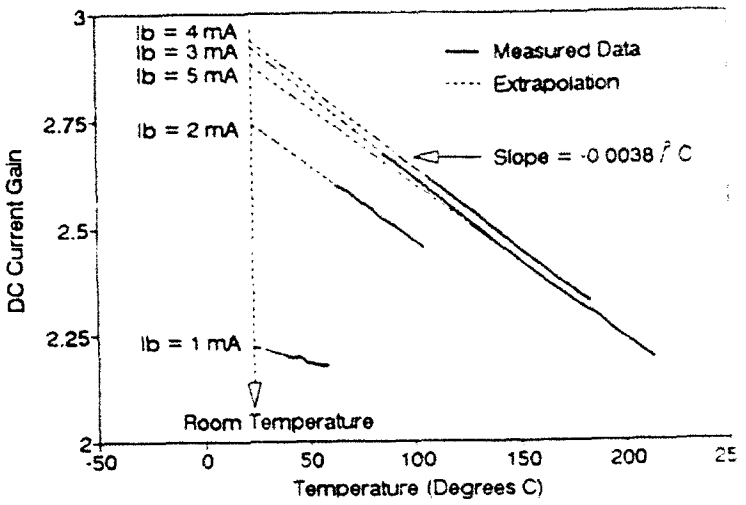

Figure 4. Gain degradation with increasing junction temperature.

2.3 Pulsed Measurements

Pulsed dc testing was also used to quantify the effects of high junction temperatures on the HBT. Pulse testing has been used to measure the I-V characteristics before the base-emitter junction temperature rises through self-heating. Base voltage pulses of 1 μs were applied at a repetition rate of 1 ms and duty cycle of 0.1%.

Figure 5 shows the circuit used to apply and measure the pulsed IV characteristics. R_1 and R_2 are used as a voltage divider in order to use the full voltage range of the source for the base emitter voltage. The series combination is also designed to match the pulse generator near 50Ω. R_b is used to measure Ib using an oscilloscope while the small capacitor C_b stabilizes ringing on the rise and fall of the base pulse. On the collector side, R_c is used to measure the collector current and C_c maintains a constant dc voltage reference.

All pulsed measurements were performed manually using an oscilloscope to ensure accuracy and base-collector current correspondence with time. The base and collector current were measured at 110 ns after the pulse edge, to avoid any rise-time effects. Figure 6 shows the significant reduction in negative differential resistance when using pulsed measurements, reflecting the device's true characteristics in the absence of self heating.

As mentioned earlier, maximum gain values in the absence of self heating can be extrapolated from the thermal measurement data of Figure 4. The pulsed measurements confirm these predicted gain values which are also indicated in Figure 6. For longer pulse widths, the amount of time required to heat the junction can be observed with this pulsed technique, where

an approximate thermal time constant of 0.5 μs has been measured.

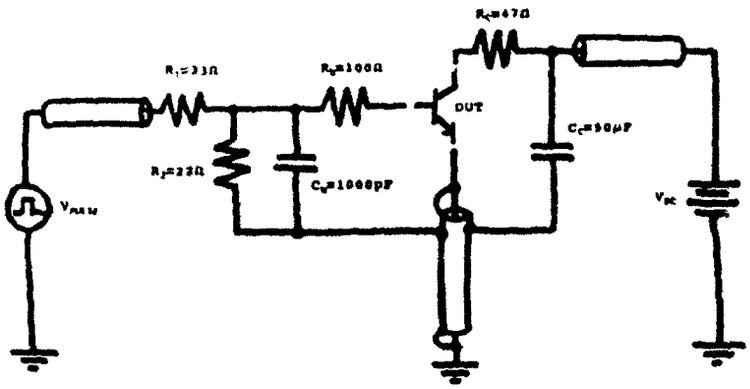

Figure 5. Pulsed measurement setup.

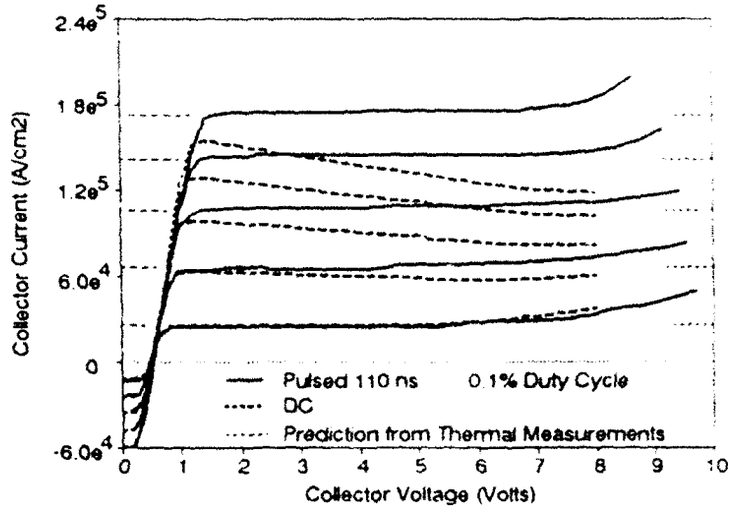

Figure 6. Pulsed vs. dc measurements.

2.4 Power and Harmonic Large Signal Transport Modeling

Figure 7 shows our HBT large signal equivalent circuit based on the Ebers-Moll model with some modifications. Seven elements are nonlinear, the base-emitter and base-collector extrinsic conductance and capacitance, and the effective current gain, β_{eff}. All nonlinear formulas are in terms of exponentials because of their efficient computation and continuous high-order derivatives.

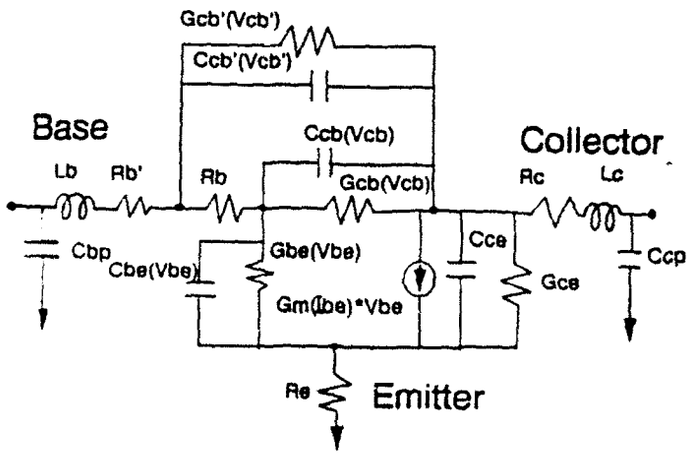

Figure 7. Equivalent circuit model for a power HBT.

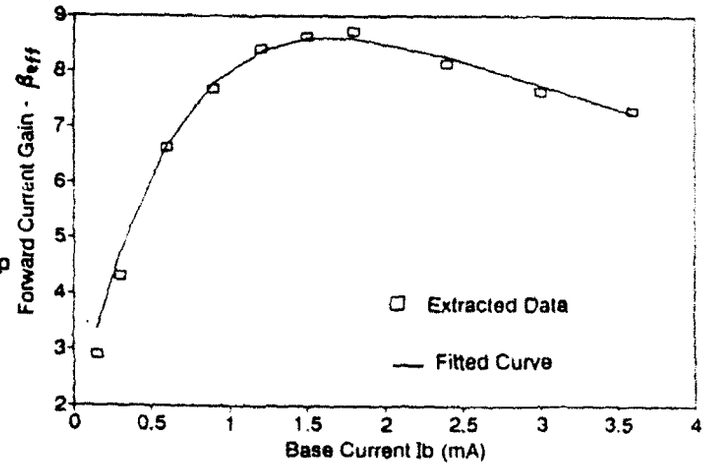

Figure 8. Fitted vs. measured current gain.

To minimize low-frequency effects due to surface traps, etc., the equivalent circuit elements were extracted solely from small-signal S-parameters over a wide bias range. An analytic procedure for direct extraction of the HBT's parasitic and intrinsic element values was

developed. The current gain, transit times and parasitic emitter and base resistance were extracted from low frequency S-parameters by a simplified equivalent circuit. The parasitic collector resistance and inductance was extracted from S-parameters at the zero collector current offset points at high base currents. The base-collector parameters were extracted from reverse-bias data. Knowing the parasitic parameter values the intrinsic parameter values were evaluated according to the equivalent circuit. Successive steps are used to fit the nonlinear function to the bias-dependent element values. Figure 8 illustrates the fitting of β_{eff} where two exponential terms are used in order to simulate the gain reduction both at high and low base currents.

This equivalent circuit model has been implemented in LIBRA, a harmonic balance simulator from EEsof Inc., and verified with 50 Ω on-wafer power measurements. The 5.5 GHz input was pulsed for 5 s at 40 KHz in order to avoid overheating due to high power dissipations. The HBT was biased in Class A with a constant base-emitter voltage which yielded a maximum RF output power level of 2 W/mm. Careful calibration was performed to account for all losses in the cables, probes and analyzer. Figure 9 shows the excellent agreement between measured and modeled output power characteristics. The fundamental output power saturates due to the output swinging from the saturation to the cutoff regions as verified by waveform simulations.

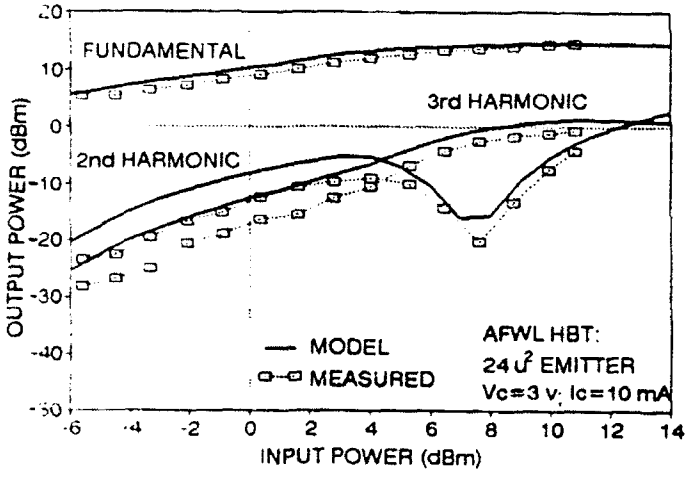

Figure 9. Simulated output power vs. power.

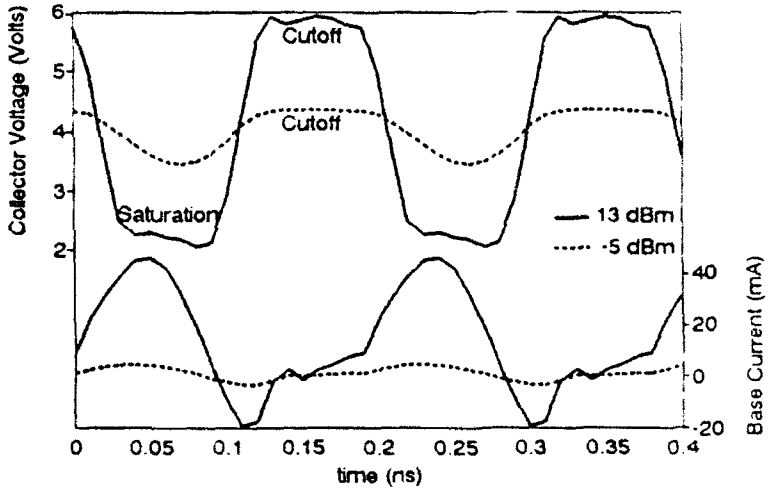

Figure 10. Simulated waveforms of nodal input currents and voltages.

Figure 10 shows the waveforms for collector voltage and base current at an input power of 5 and 13 dBm. The collector voltage is clipped at both the top and bottom when the HBT swings into saturation and cutoff. In addition to causing power saturation, this also causes the second and fourth harmonics to approach a minimum while the third harmonic approaches a maximum. The waveforms also show that the base current swings negative before it settles to a small cutoff value indicating a relatively large amount of stored charge that must be depleted before the base-emitter voltage becomes negative. Likewise we have found a relatively large base-emitter transit time for this HBT of 5 ps.

2.5 Large Signal Thermal Modeling

In this same transport model, the thermal effects described earlier are also included. These effects include the linear decrease in V_{bc} with temperature as seen n Figure 1, and the linear gain degradation with temperature as seen in Figure 4. In the model, the transient temperature of the device is calculated based on the total power dissipated, the thermal resistance, and the thermal time constant. Results of the large signal model have been compared to pulsed and dc measurements as seen in Figures 11, 12, and 13. An additional useful product of this model is the determination of the actual junction temperature as seen n Figure 14 for a pulsed simulation. Because of the long time constant, the microwave CW operation simply causes a constant junction temperature with time, and the model adjusts the I-V relationships accordingly. The model s useful for simulating device characteristics with different heat-sink configurations, allowing the use of on-wafer measurements to predict packaged device performance. The model also gives an indication of the thermal limitations of the device in all modes of operation including dc, pulsed and RF.

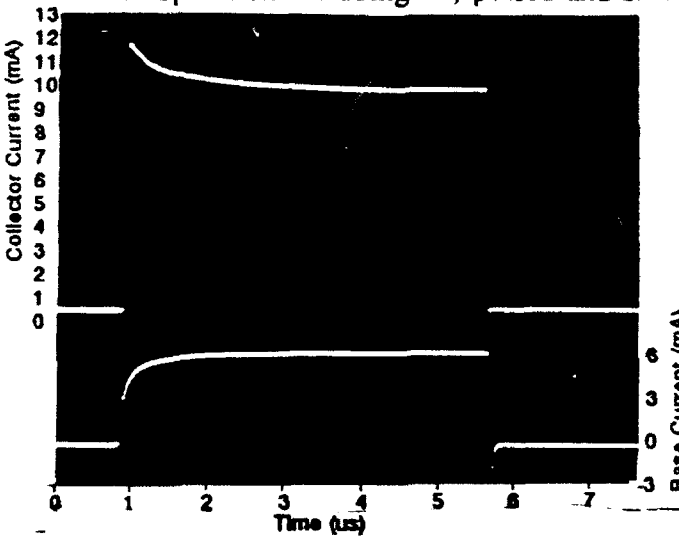

Figure 11. Measured response of I_b and I_c to a 5 μs base voltage pulse.

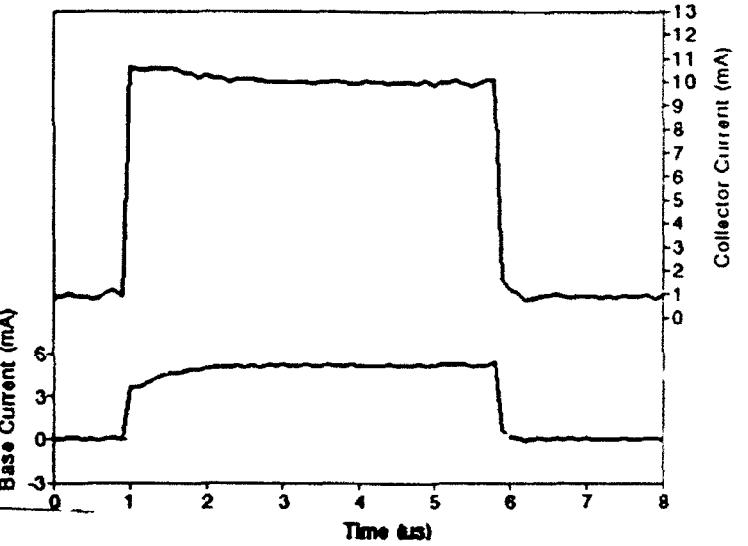

Figure 12. Simulated response of I_b and I_c to a 5 μs base voltage pulse.

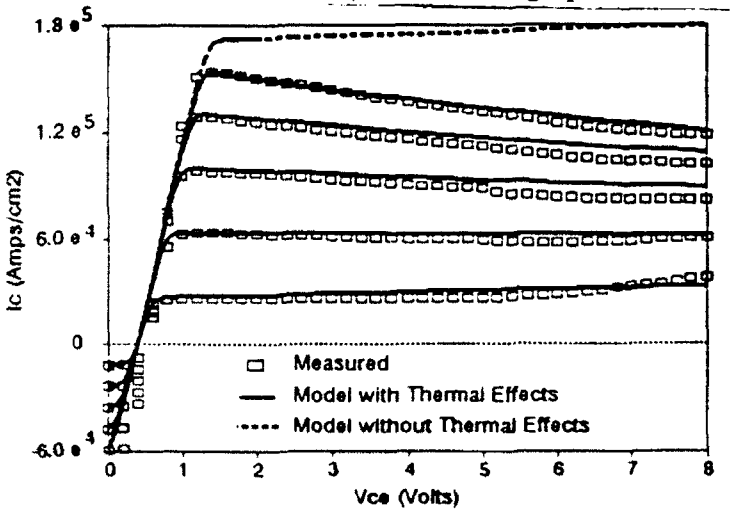

Figure 13. Simulated and measured HBT collector characteristics.

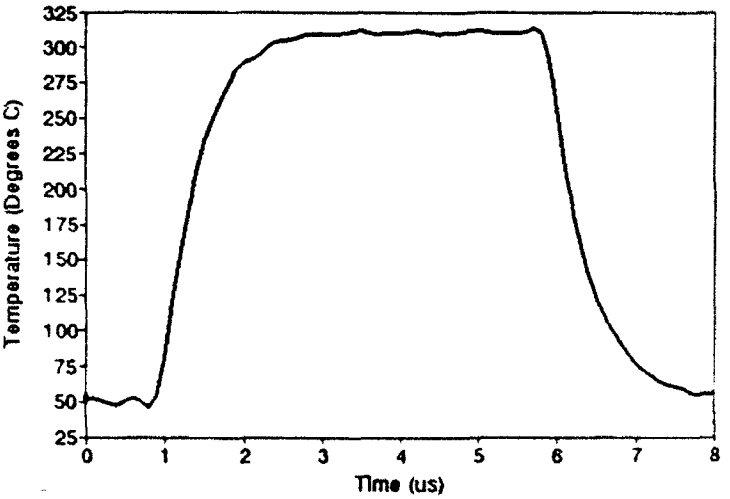

Figure 14. Modeled junction temperature during the simulation of Figure 13.

2.6 Thermal Effects on Microwave Performance

2.6.1 Experimental

To investigate the variation of microwave parameters with temperature, a variable-temperature measurement system was constructed. With this system, S-parameter measurements were performed on a device at temperatures varying from room temperature to 226°C. The measurement system consists of an HP8510B network analyzer to perform the S-parameter measurements, an HP4142B to supply the variable dc bias, Gore-Tex flexible cable, Tektronix coplanar on-wafer probes and, a West-Bond hot chuck.

The chip containing the test device was bonded to a TO-3 package by high-conductivity silver epoxy ($\sigma \approx 1 \times 10^4 / \Omega cm$). Heat sink compound was applied to the back side of the TO-3 package and then bolted to the hot chuck. A simple two-fin heat-shield was attached to the probes to reduce probe-body heating via convection and radiation from the hot chuck. Even with these heat shields, the probe body, as well as a portion of the Gore cable, heats up during measurements. Tektronix and Gore confirm that these components can withstand temperatures up to 150°C and 75°C respectively, but since the electrical characteristics of these components change with temperature, calibrations must be performed often.

Full two-port on-wafer calibrations were performed before each set of S-parameter measurements at a particular temperature. The short-open-load-thru (SOLT) type calibration was performed using a Tektronix Tek-96 on-wafer calibration substrate. The dc resistance of the 50 Ω load standard was measured and utilized in the calibration at each temperature. This resistance, however, only changed by 0.8 Ω over the 200°C range.

To measure the actual ambient temperature presented to the device under test, the diode characteristics of a neighboring HBT were monitored. The base and emitter of this HBT were wire-bonded to leads, and while applying a small constant base current, the base-emitter voltage(V_{be}) was measured periodically during the entire testing sequence. Since the diode characteristics are very sensitive to temperature, the actual wafer temperature can be easily calculated by using previously calibrated V_{be} versus temperature characteristics.

For the particular series of S-parameter measurements to be described, a wide range of temperatures and bias conditions were implemented. The ambient wafer temperatures were calculated to be 23, 84, 123, 171, and 226°C. This covers the typical range of junction temperatures encountered during normal device operation. Actual junction temperature is evaluated later using thermal resistance and dissipated power. At each of the five temperatures, S-parameter measurements were taken at 28 bias points as shown in Figure 15. These bias points cover many regions of operation including forward active, saturation, cutoff, negative I_c, and the $I_c=0$ point. This range of bias values was chosen to enable the full characterization of the major physical mechanisms which contribute to the HBT characteristics.

2.6.2 Theory and Analysis

Before developing a large signal model, it is necessary to establish the dynamic behavior of various device elements with bias and temperature. The technique used in this work was to measure and model the microwave characteristics at many bias points and many temperatures. Microwave parameters were extracted for a simple equivalent circuit from the measured S-parameter data. To aid in the interpretation of these element values with bias and temperature, a physical model based on material parameters and geometry was used to calculate theoretical values.

Of course, all parts of the HBT are expected to be affected by temperature, but the base-

emitter diode and the current gain are known to have the most significant change with temperature. Therefore, the microwave elements corresponding to these areas are analyzed most extensively.

A. Bias- and Temperature-Dependent Equivalent Circuit

The microwave equivalent circuit used for this temperature investigation is the simple Pi-model shown in Figure 16. This equivalent circuit, which treats all areas of the HBT with lumped elements, was found to match the HBT characteristics up to 10 GHz in all bias conditions. R_{eb} and C_{eb} model the base-emitter diode, R_{cb} and C_{cb} model the base-collector diode, g_m is the transconductance, and R_{ce} is the output resistance. R_b, R_c, and R_e are parasitic contact and bulk resistances, and C_{ec} is the emitter-collector metalization crossover capacitance.

At each bias point, for each temperature, a unique set of equivalent circuit element values were extracted. Initial element values were calculated by using a one-dimensional physical model based on material properties and dc measurements. This model is described in the next section. From these initial values, the circuit simulator LIBRA, was used to optimize all element values to fit the measured S-parameter data. Element values determined from this equivalent circuit are termed 'measured' throughout this work but are actually *extracted values* from measured S-parameters.

B. One-Dimensional Physical Model

The one-dimensional physical model used for this work is based on standard semiconductor physics with particular attention to temperature dependencies. The terminal currents are calculated from first principles using device dimensions, material properties, junction temperature, and applied voltages. The temperature dependence of many of the material properties for both GaAs and AlGaAs were included in this physical modeling. These include the bandgap, Eg, the intrinsic carrier concentration n_i, the saturation velocity, v_{sat}, the emitter electron mobility, μ_{ne}, the base hole mobility, μ_{pb}, and the collector electron mobility, μ_{nc}. The actual calculations are performed in a spreadsheet which provides ready assess to all calculations of material parameters and flexibility to add additional analyzes without full recalculation. The capability for including self-heating and constant current boundary conditions are implemented using the spreadsheet to solve the interdependencies.

In the model there is room for a limited amount of fitting by changing the surface and bulk recombination velocity and lifetime for the model since these values are very process dependent and difficult to predict theoretically. In addition, the parasitic resistances (R_b, R_c, and R_e) which are used for the model calculations are measured values from dc analyses. These resistances did deviate from attempted model predictions probably due to misalignment and over-etching during processing.

Several standard assumptions have been made for the model calculations. First, all material is assumed to have uniform doping and composition with abrupt junctions. This assumption is quite accurate, since the device was designed to be uniform and abrupt by using MBE growth. The commonly used depletion approximation and quasi-neutrality were also assumed.

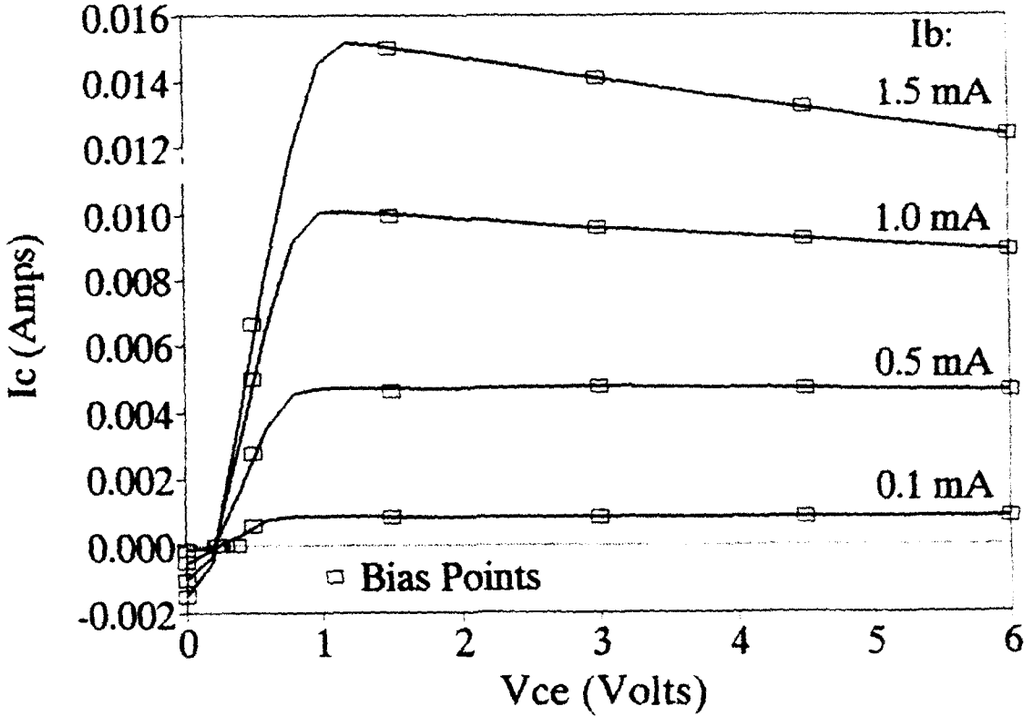

Figure 15. Bias points used for elevated temperature S-parameter measurements.

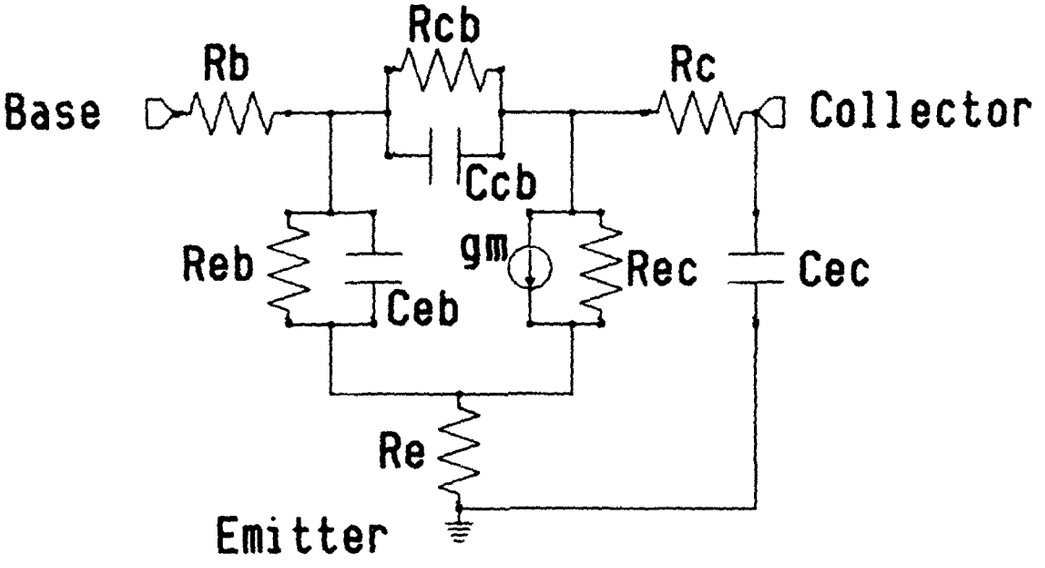

Figure 16. Microwave equivalent circuit used for bias- and temperature-dependent parameter extraction up to 10 GHz.

Maxwell-Boltzmann statistics were applied assuming a linear gradient of holes in the quasi-neutral base, resulting in the Shockley equation for the emitter-collector transport current. This current is a function of the internal V_{be} which does not include the base and emitter parasitic resistance effects. These effects are included afterwards. High level injection (velocity saturation), the Kirk effect (base push-out), and Shockley-Reed-Hall (SRH) recombination in the base were also included in this emitter-collector current. For the base-emitter current, which is also a function of the internal V_{be}, SRH bulk recombination and reverse hole injection were included, both having an $e^{(Vbe/kT)}$ dependence. Also included was surface and depletion region recombination, both with an $e^{(Vbe/2kT)}$ dependence. In addition, the model includes the base-collector diode transport current which is a function of the internal V_{cb} and temperature.

Once the terminal currents are calculated from internal voltages, the actual *terminal* voltages are evaluated accounting for the parasitic R_c, R_b and R_e. As a second order effect, the external pad to pad leakage resistance was included ($R \approx 500$ MΩ). This strictly measured quantity effects only the low V_{be} characteristics, and is probably due to substrate and surface leakage.

Device self-heating is included by using a measured thermal resistance which is assumed to remain constant with temperature. The junction temperature is used for all calculations of material properties and transport equations, iterating until the equations are self-consistent.

Several microwave parameters are calculated from two sets of I-V characteristics with slightly offset V_{be}. The small signal base-emitter resistance is given by

$$R_{eb} = \frac{\Delta V_{be}}{\Delta I_b} \tag{1}$$

For a constant V_{be}, I_b will increase exponentially with temperature (T). Therefore, for a given change in V_{be}, the change in I_b will increase causing R_{eb} to decrease exponentially with T. The transconductance is

$$g_m = \frac{\Delta I_c}{\Delta V_{be}} \tag{2}$$

and for similar reasons will increase exponentially with T. C_{eb} is given by the slightly more involved expression:

$$C_{eb} = C_{je} + g_m \tau_b \tag{3}$$

and can be shown to increase with T.

2.6.3 Results and Discussion

Both the dc I-V characteristics and the microwave element values have been calculated using the physical model for all measured temperatures and bias points. A comparison of I-V characteristics confirms the validity of the model and indicates the magnitude of possible error. A comparison of calculated and measured microwave elements confirms the accuracy of the equivalent circuit extraction and the degree to which the bias- and temperature-dependence of

these elements agrees with device physics predictions.

A. I-V Characteristics

To test the agreement of the physical model to the measured results, first the dc I-V characteristics were compared. Figure 17 shows this comparison between the measured and modeled base and collector currents (Gummel plot) for the two extreme temperatures measured, 23°C and 226°C. The slope of I_c in the log-linear region is proportional to $e^{(Vbe/kT)}$, while the slope of I_b is approximately proportional to $e^{(Vbe/2kT)}$. As described in the last section, the 2kT dependence is due to the surface and depletion region recombination current. The surface recombination velocity and bulk recombination lifetime were adjusted to improve the fit for the 23°C curve and were assumed to be temperature independent. At high V_{be}, both I_c and I_b show a saturation due to the series base and emitter resistances. At low V_{be} a pad to pad resistive leakage dominates over the diode transport current and causes the flattening of the characteristics.

Since the base-collector currents are also accounted for in this model, the collector current characteristics versus collector voltage can be calculated. Figure 18 shows a comparison of measured and modeled room temperature collector characteristics. The measured points correspond to bias points for subsequent S-parameter measurements. Figure 19 shows the corresponding V_{be} characteristics. Likewise Figure 20 and 21 show the collector and corresponding base-emitter characteristics for the 226°C measurement.

A constant base current boundary condition is used for each series in these calculations. Since calculating I_b and I_c are based on a given V_{be}, the value of the base current boundary condition is modified to correspond to an actual measured V_{be}. Therefore, for the model calculations, the value of this constant I_b for each series is slightly different than the applied I_b values of the measurements. The I_b values differ by less than a factor of two for all calculations. In this way, the most accurate results can be obtained when considering the error in *both* the base-emitter characteristics and the collector characteristics. Even so, much of the error between modeled and measured appears in the collector characteristics. The error in the magnitudes of I_c is due to the accumulation of errors in input material parameters which is analyzed in detail for the microwave elements in a following section.

The model also includes self-heating, accounting for the decrease in I_c and V_{be} with increasing collector voltage seen at all temperatures. Figure 22 shows the modeled junction temperature corresponding to the calculations in the previous four figures. It can be seen in Figure 18 that the slopes of the room temperature collector characteristics are different than those of the measurements. This is due to the fact that the model uses a thermal resistance which is assumed constant with temperature. The thermal resistance value is measured as one average value over the whole temperature range of interest when actually the thermal resistivity increases with temperature. The overall result is that the thermal resistivity for the model is high for the room temperature case, causing the model to predict a more dynamic temperature change with power, and causing the collector characteristics to change more dynamically than the measured result.

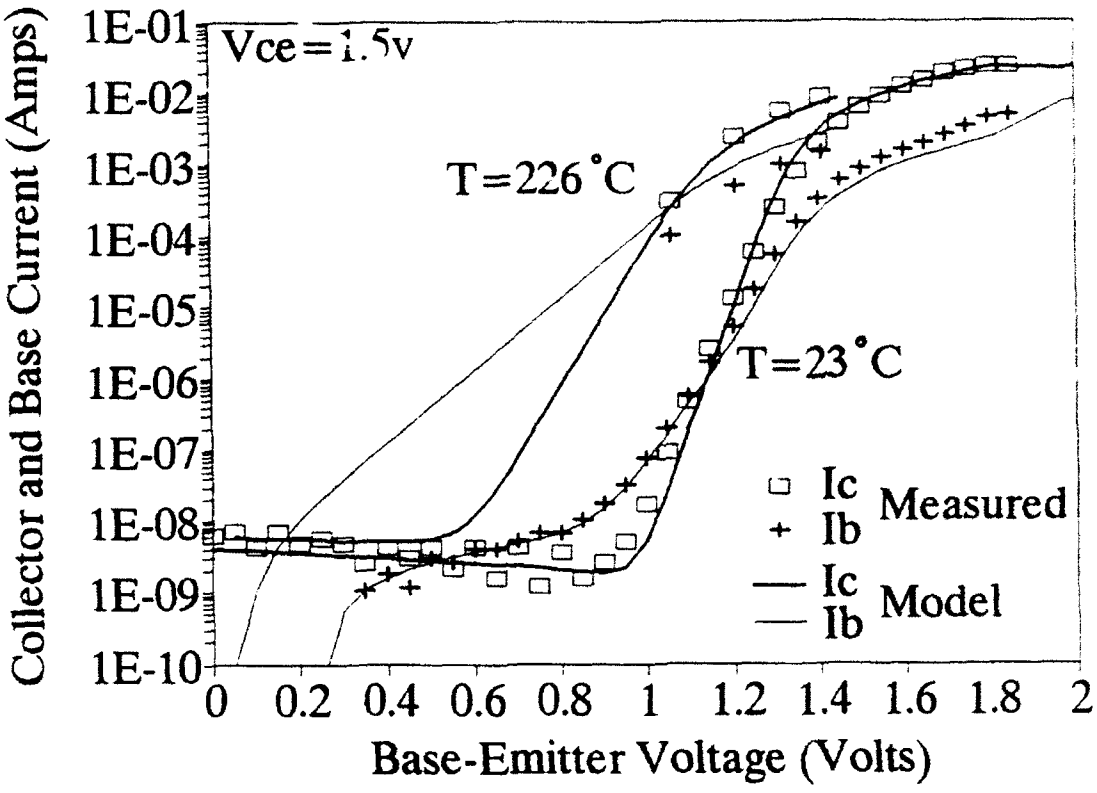

Figure 17. Measured Base and Collector currents along with physical model calculations for the HBT at two ambient temperatures.

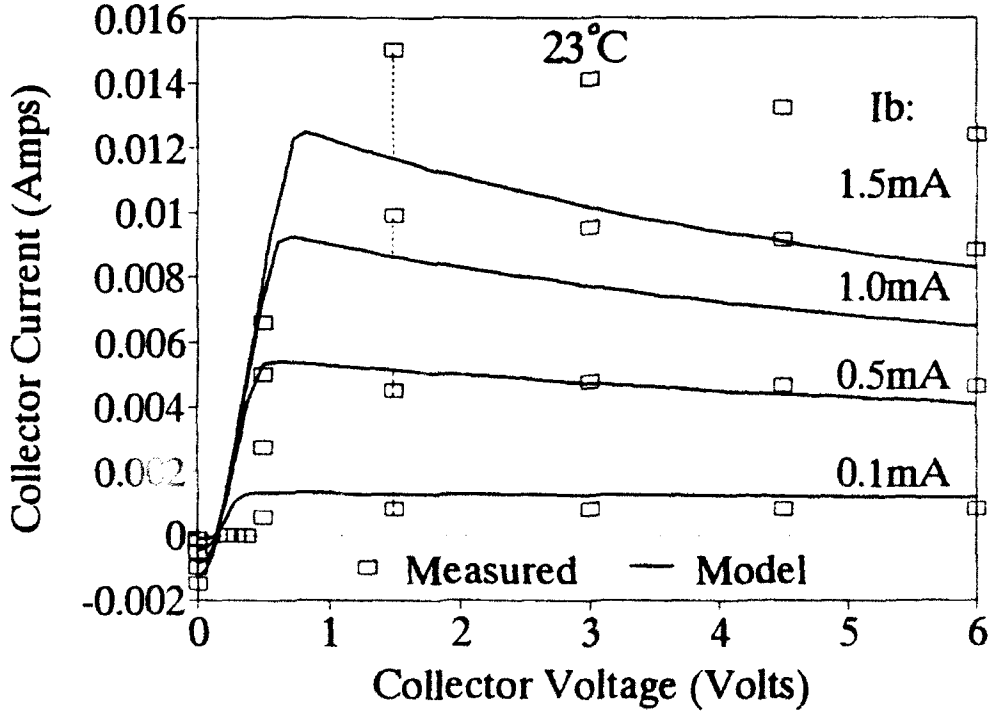

Figure 18. Physical Modeling of room temperature collector characteristics.

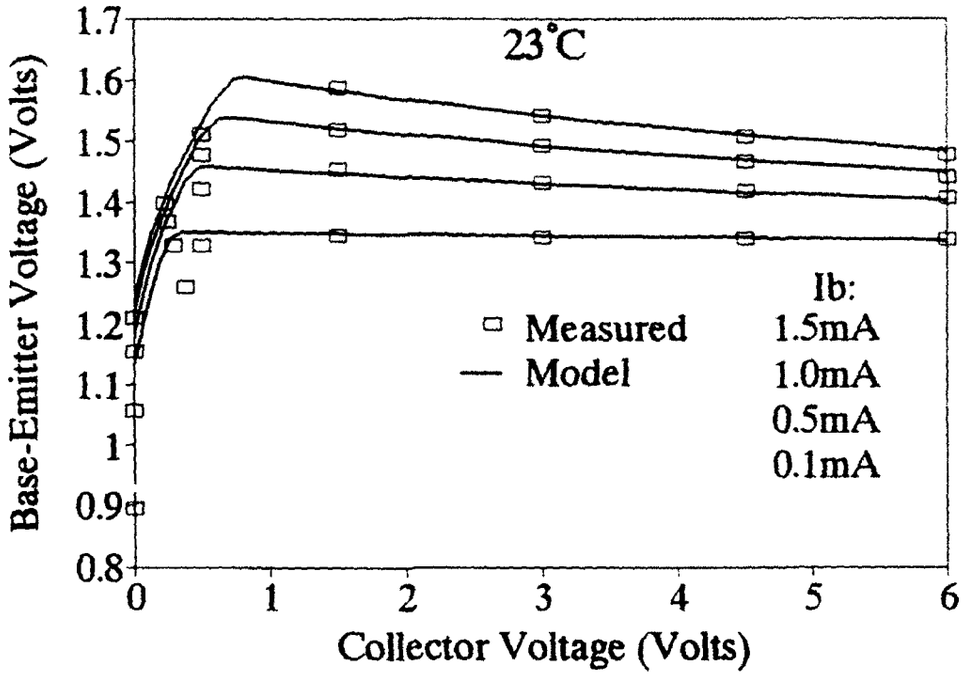

Figure 19. Physical modeling of base-emitter voltage associated with the collector characteristics of Figure 18.

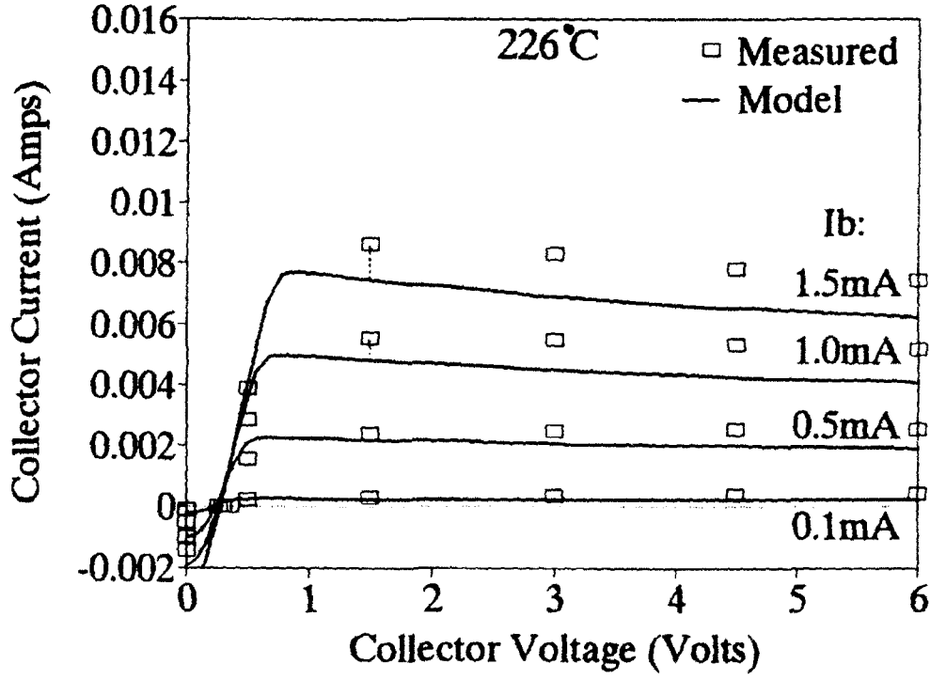

Figure 20. Physical modeling of collector characteristics at 226°C.

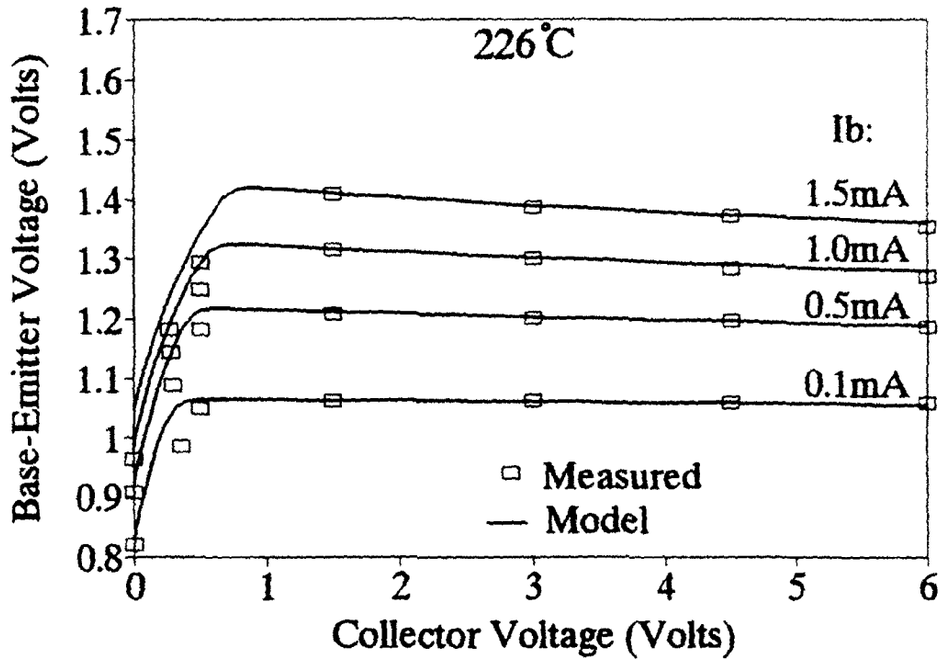

Figure 21. Physical modeling of base-emitter voltage associated with the collector characteristics of Figure 20.

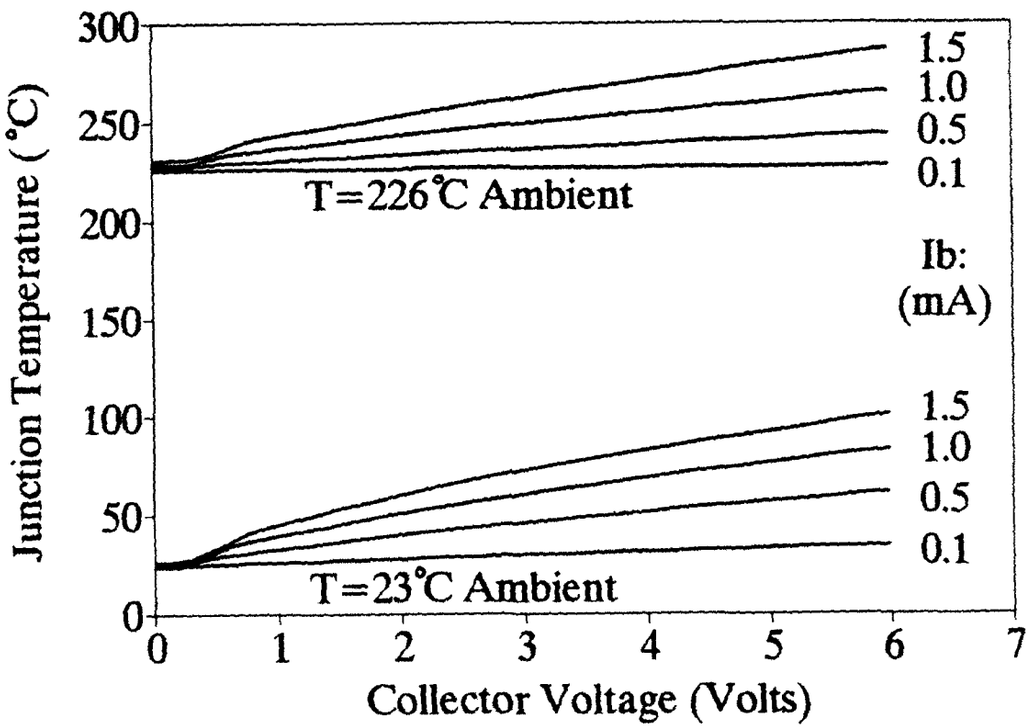

Figure 22. Junction temperatures calculated by the physical model for the previous room temperature and 226°C simulations, Figures 18-21.

B. Microwave Circuit Elements

For a complete comparison to the measured element values (derived from the S-parameters), the model was evaluated at all five measurement temperatures. Figure 23 shows an enlarged view of the Gummel plot of Figure 17. This plot shows the measured and modeled base and collector currents at all measurement temperatures. The model tends to show more I_c saturation than the measured I_c while the opposite is true for I_b. This difference also shows up in the calculations of microwave elements, and is probably due to the lumped approximation for the parasitic base and emitter resistances.

Figure 24 shows the temperature dependence of R_{cb} versus V_{be} corresponding to the same bias points in Figure 23. As described previously, R_{cb} is expected to decrease with temperature because of the larger change in I_b at high temperatures for a given change in V_{be}. The saturation effect as V_{be} increases is caused by the parasitic R_b, and R_e taking up an increasingly larger portion of the applied external V_{be}. As a result, the actual internal diode V_{be} does not increase as quickly in this region. In the absence of this saturation, R_{cb} decreases by an average of 1.3% per°C indicating the change at a constant *internal* V_{be}. This change is simply an average since the exact magnitude of change depends on the particular bias region and temperature as seen in the figure.

Figure 25 shows g_m for the five temperatures and shows the expected increase with temperature for a given V_{be}. Again, in the absence of saturation, g_m increases by an average of 1.4% per°C. Since the current gain is defined as $\beta = R_{cb}g_m$, β will increase slightly with temperature at constant V_{be}. Normally, however, the current gain is analyzed as a function of constant I_b. At constant I_b, V_{be} decreases with temperature as seen in Figure 19. The net result, as evidenced by the negative differential resistance in the I-V plots of Figure 18 and 20, is that current gain decreases with temperature.

Figure 26 shows the components of modeled C_{eb} along with the measured values at room temperature. For all of the bias points measured it can be seen that the diffusion capacitance dominates. Diffusion capacitance is due to the enhanced distribution of minority charge in the base during the forward bias condition and is expected to increase with temperature as shown in Figure 27. In the absence of saturation, C_{eb} increases by an average of 0.8% per°C.

C. Error Analysis

There is a certain error in the absolute magnitude of the model calculations. This is due to the accumulated error from the large number of material parameters used as inputs. These parameters such as the mobility, bandgap, and intrinsic carrier concentration are formulas fit to measured data and therefore have some error. To quantify the effect of these accumulated errors, the model has been evaluated assuming a worst-case $\pm 40\%$ error in each material parameter. Figures 28 through 30 show this accumulated error for the considered microwave elements at room temperature. It can be seen that the absolute magnitudes of the model calculations are reasonable. In an absolute sense the error can be large, however the trends predicted by the model are consistent.

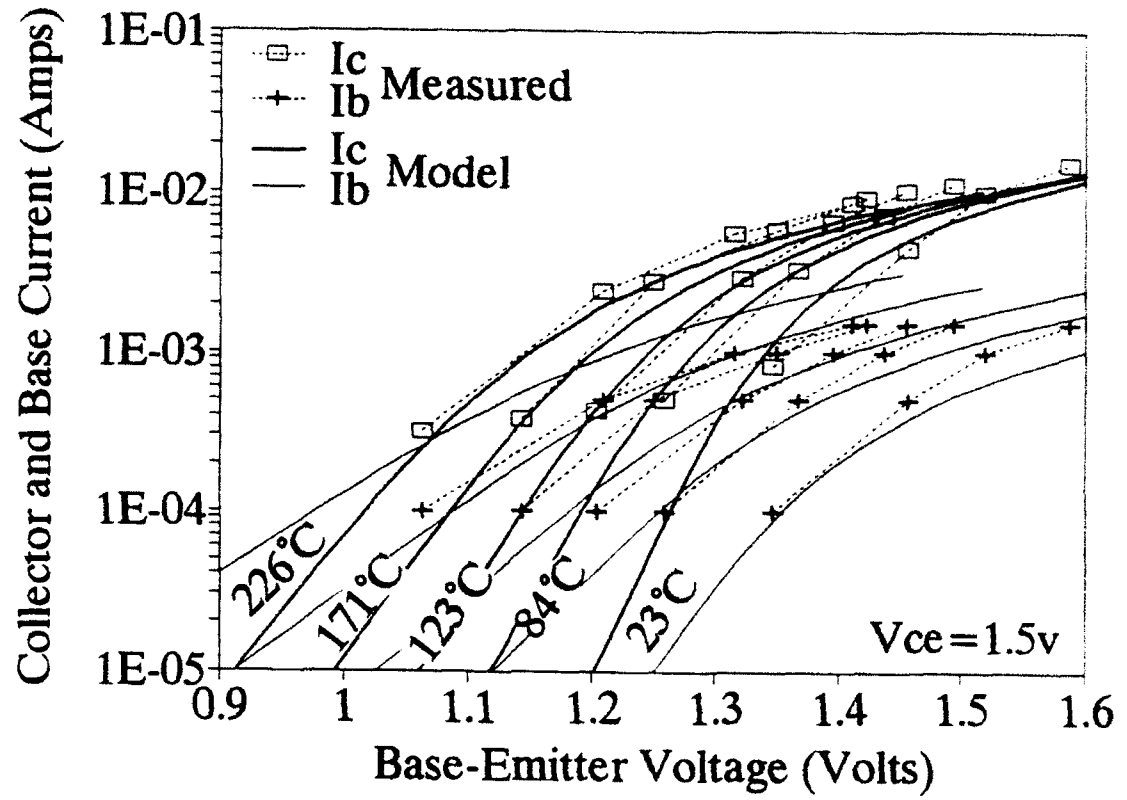

Figure 23. Gummel plot of base and collector currents including physical model calculations and measurements at all evaluated temperatures.

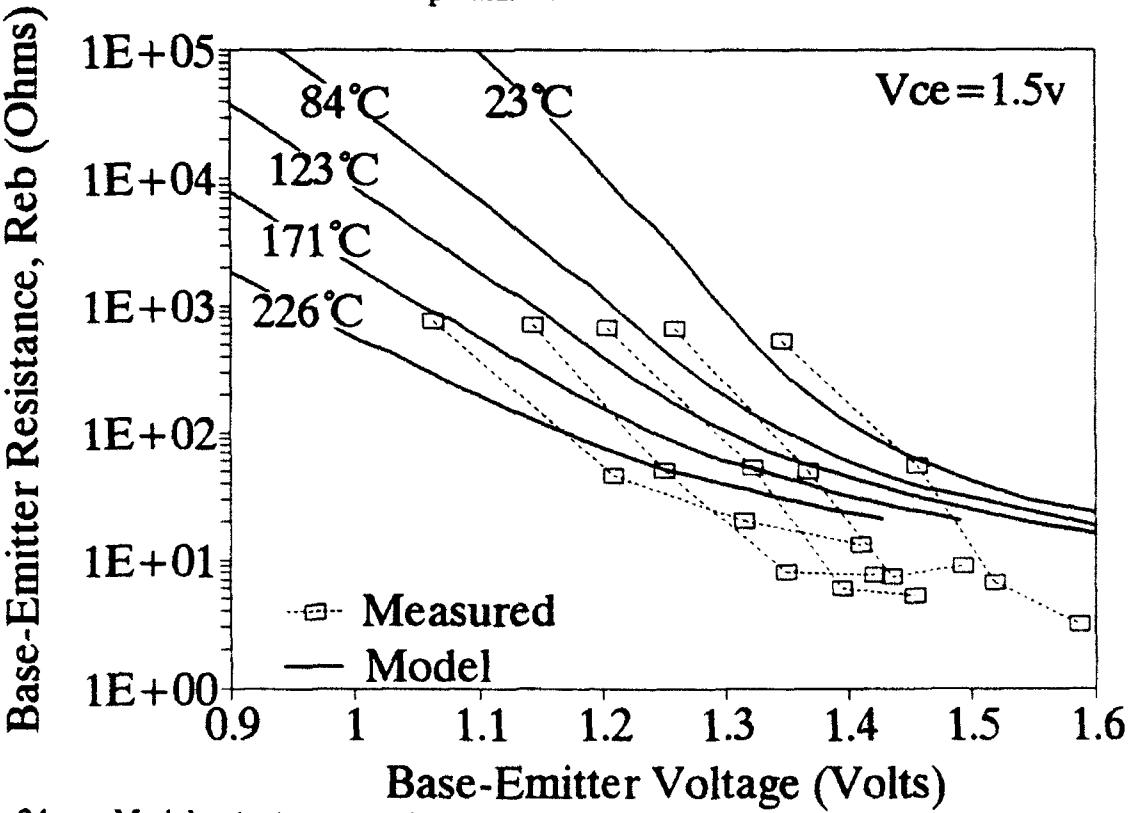

Figure 24. Model calculations and measurements of the base-emitter resistance, R_{eb}.

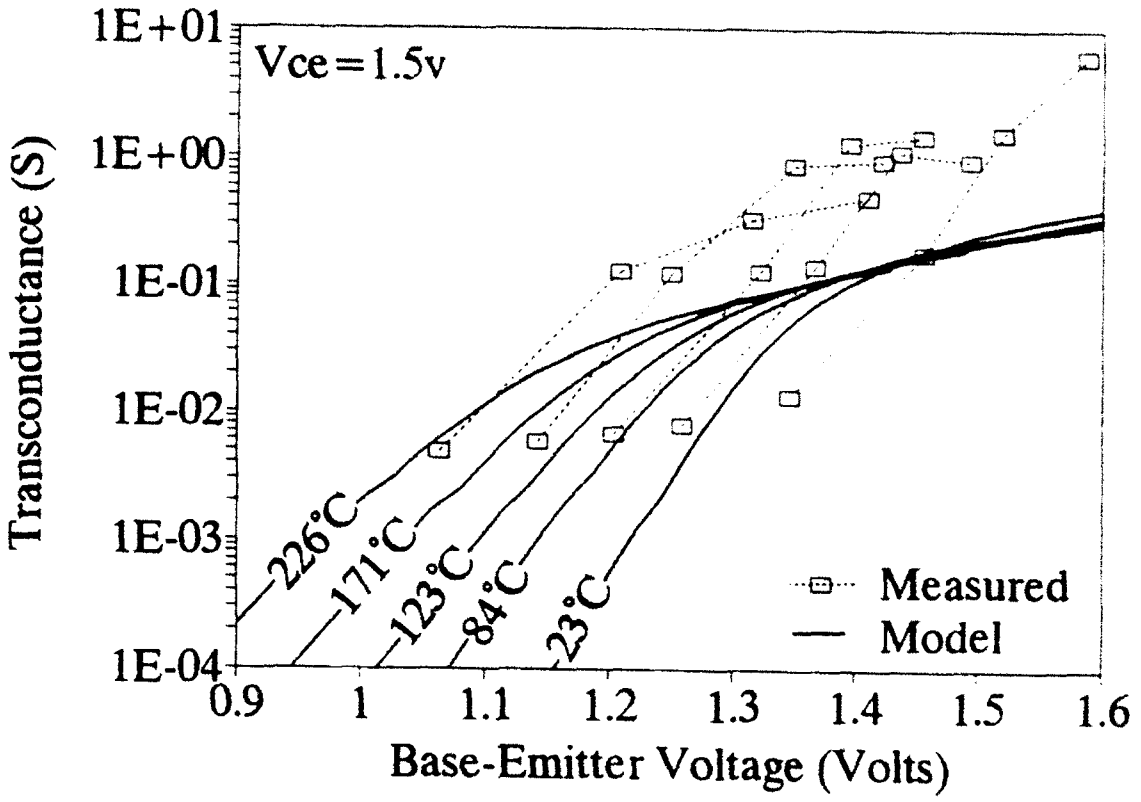

Figure 25. Model calculations and measurements of transconductance, g_m.

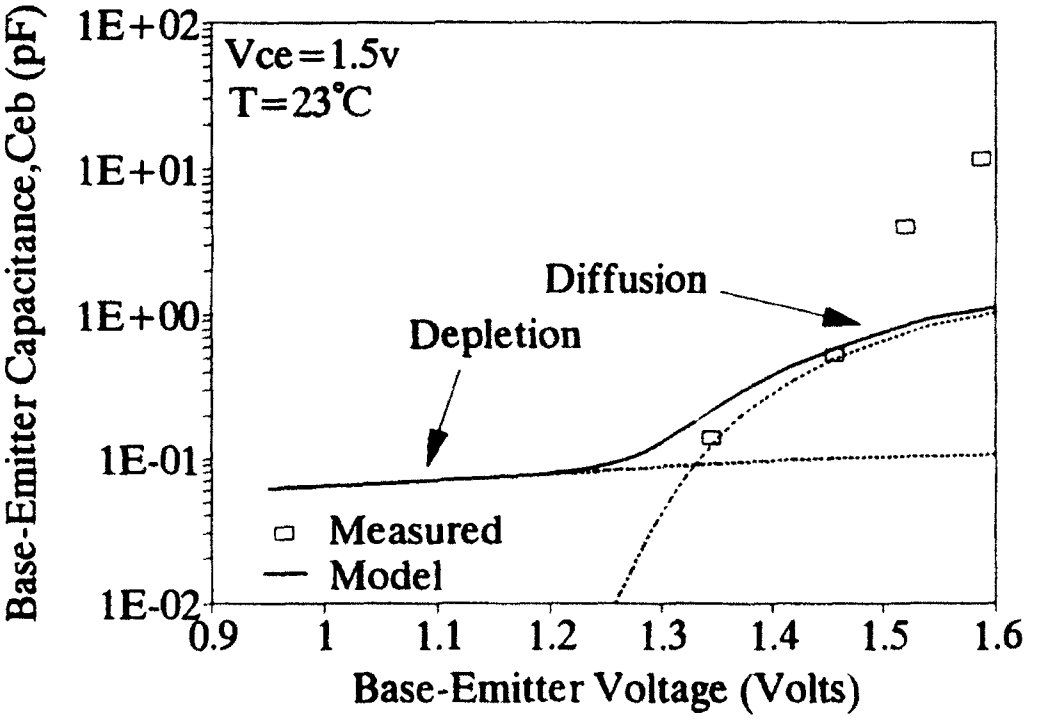

Figure 26. Model calculation of base-emitter capacitance showing depletion and diffusion components.

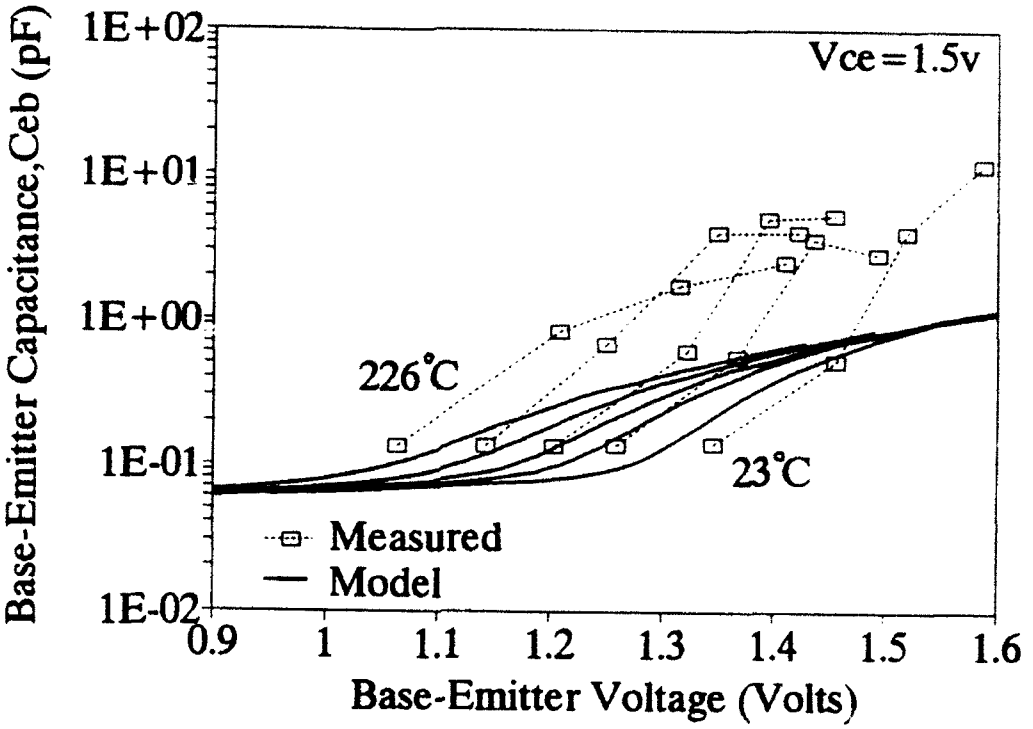

Figure 27. Model calculations and measurements of the base-emitter capacitance, C_{eb}.

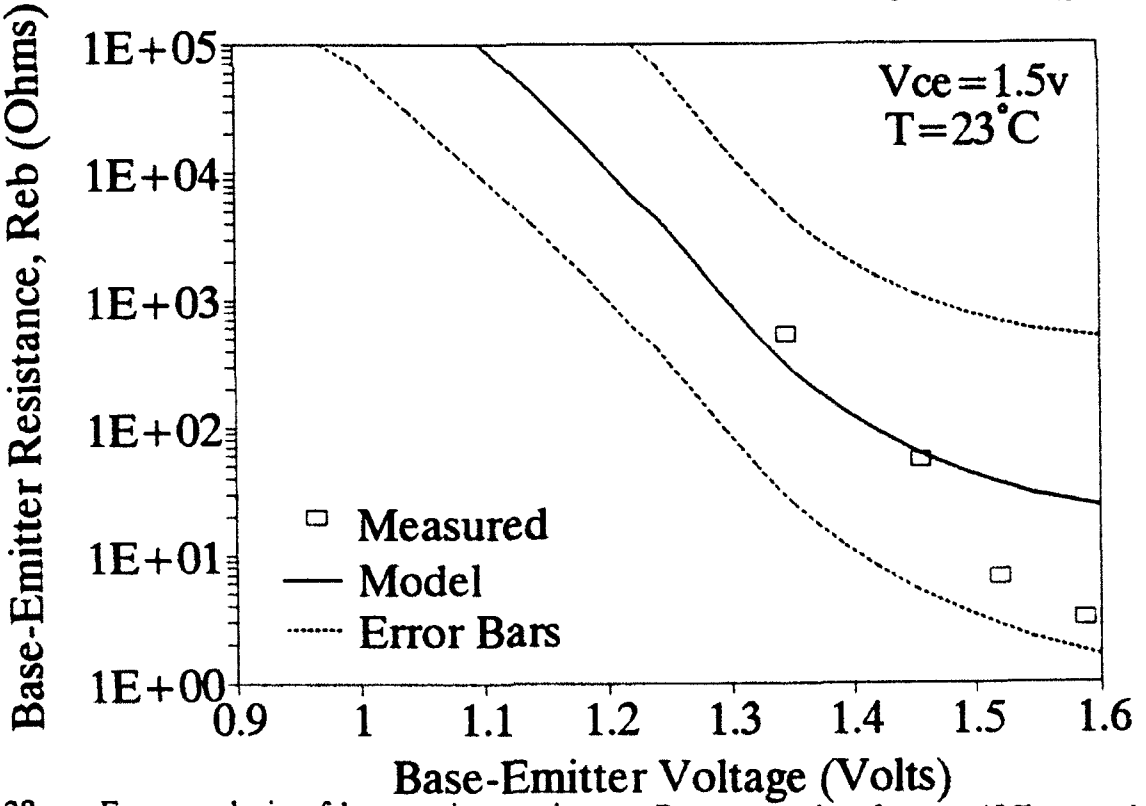

Figure 28. Error analysis of base emitter resistance R_{eb}, accounting for a ±40% error in physical constants used for the physical model calculations.

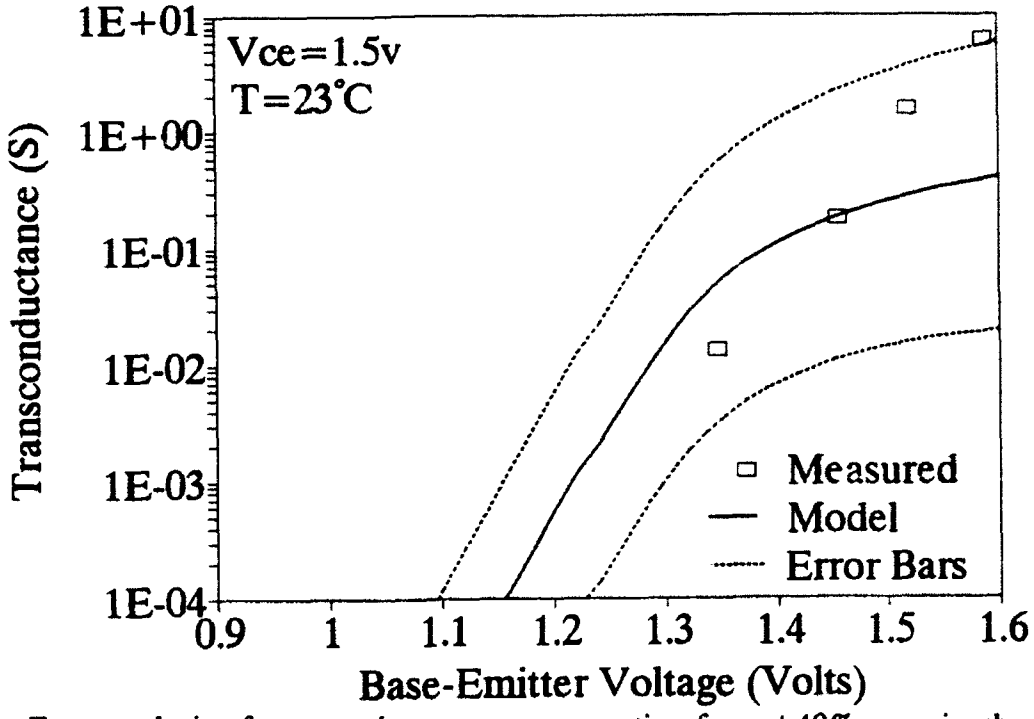

Figure 29. Error analysis of transconductance g_m, accounting for a ±40% error in physical constants used for the physical model calculations.

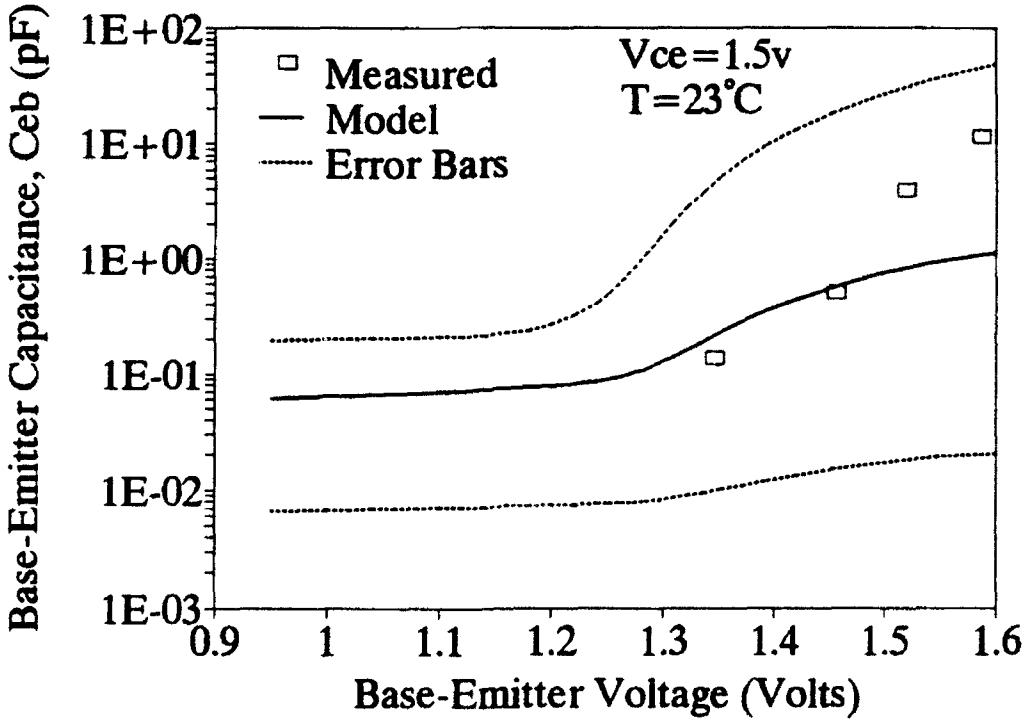

Figure 30. Error analysis of base emitter capacitance C_{eb}, accounting for a ±40% error in physical constants used for the physical model calculations.

D. Transit Times and Cutoff Frequencies

A useful measure of the overall high frequency performance of a transistor is the unity gain cutoff frequency, f_T, and the maximum frequency of oscillation, f_{MAX}. These values can also be estimated from circuit theory and device physics as

$$f_T = \frac{1}{2\pi\tau_{ec}} \tag{4}$$

$$f_{MAX} = \sqrt{\frac{f_T}{8\pi R_b C_C}} \tag{5}$$

where the transit times are

$$\tau_{ec} = \frac{V_T}{I_c}(C_{eb} + C_{bc}) + \tau_b + \frac{X_d}{2V_{sat}} + R_c C_c \tag{6}$$

$$\tau_b = \frac{W_b^2}{2V_T \mu_{nb}} + \frac{W_b}{v_{sat}} \tag{7}$$

V_T is the thermal voltage (kT/q), C_c is the total collector capacitance ($C_{ce}+C_{cb}$), and X_d is the base-collector depletion width.

There are several terms in τ_{ec} which produce conflicting effects with increasing V_{be} bias and increasing temperature, but the overall effect for τ_{ec} is to decreases with increasing V_{be} bias due to the exponential increase in I_c. In response, f_T increases with bias. Both f_T and f_{MAX} have been calculated and measured for the HBT in the previous analysis at all the bias points and are shown in Figures 31 and 32. There is a discrepancy between the overall magnitudes between the measured and model due to the model uncertainty described earlier. However, the trends agree well, in both direction and magnitude of change.

Figure 33 and 34 show the same f_T and f_{MAX} data plotted as a function of temperature for constant I_b. Again, the relative magnitude and direction of change agree well, indicating a drop in f_T of approximately 0.2% per°C and a drop in f_{MAX} of 0.3% per°C. The added temperature dependence of f_{MAX} is due to the increasing parasitic base resistance with temperature. These percentage drops in cutoff frequencies are useful for estimating the temperature dependence for other devices at varying power dissipation levels and varying ambients. In addition, these values show qualitative agreement with others' strictly numerical modeling work and a report on low-temperature HBT measurements.

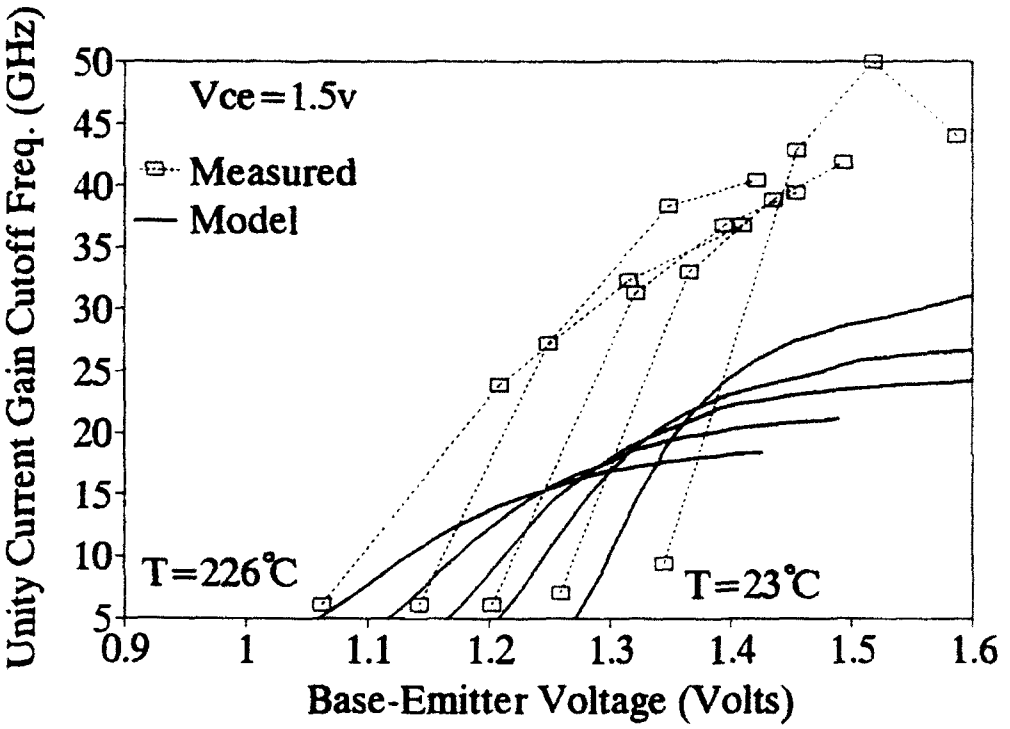

Figure 31. Model calculations and measurements of unity gain cutoff frequency, f_T.

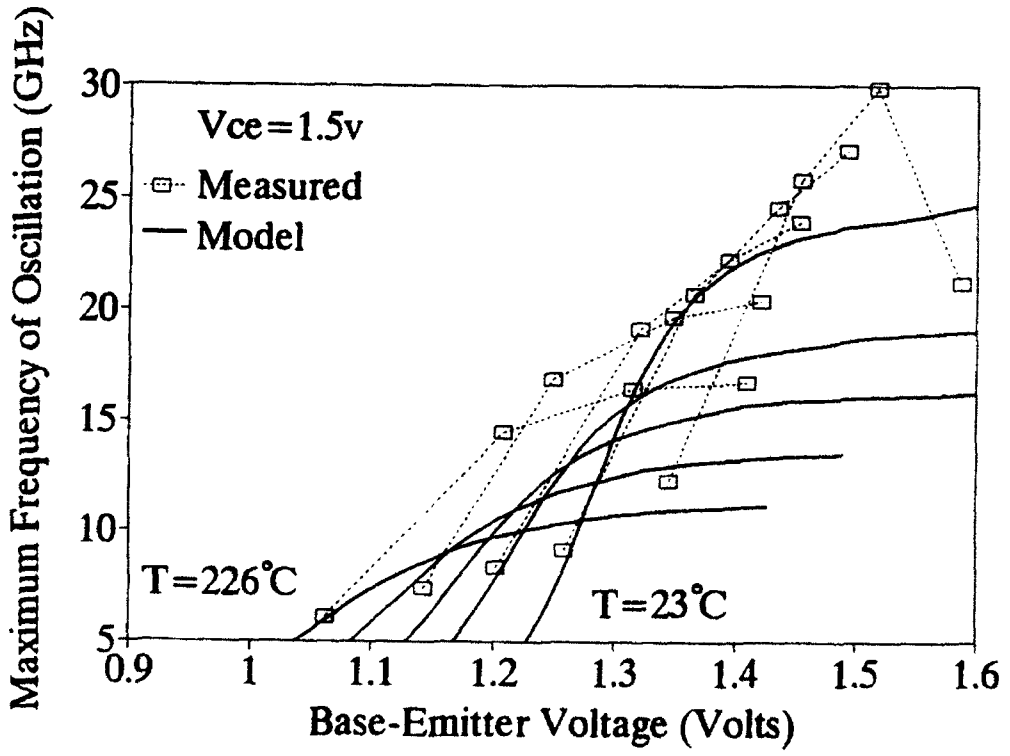

Figure 32. Model calculations and measurements of maximum frequency of oscillation, f_{MAX}.

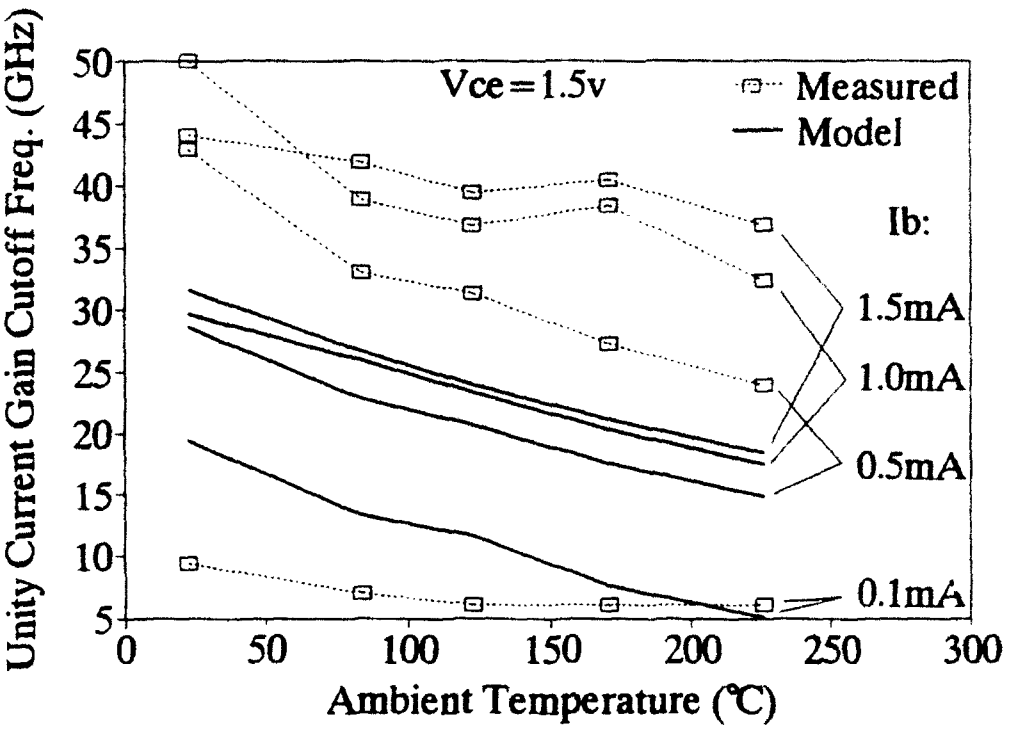

Figure 33. Measured and modeled unity gain cutoff frequency, f_T, as a function of temperature.

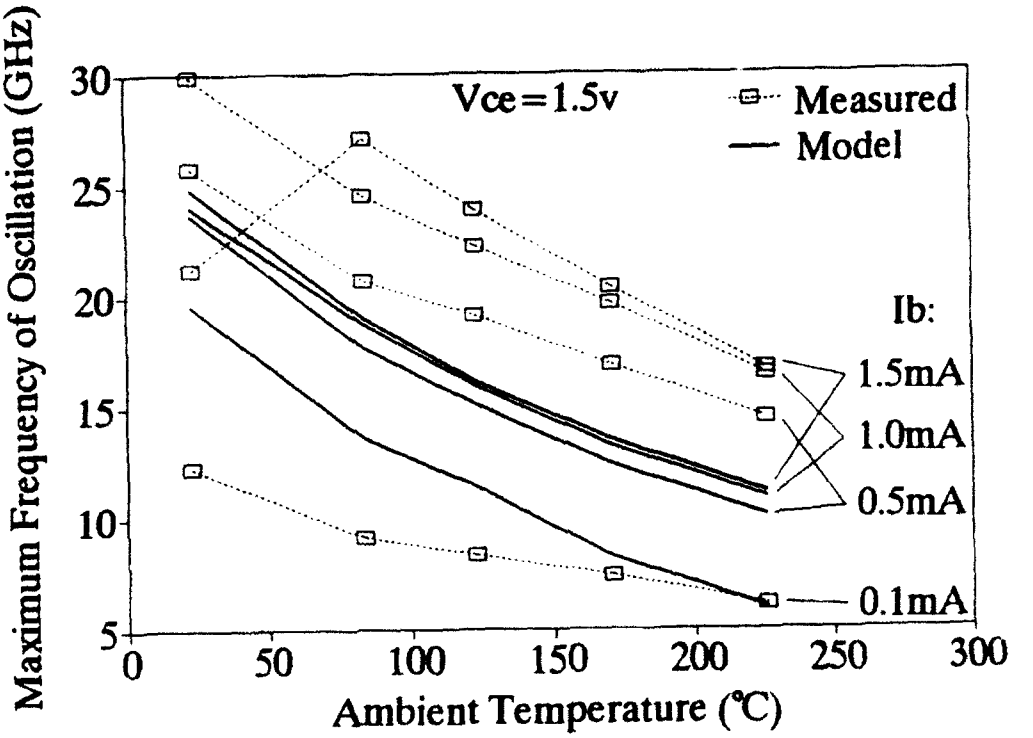

Figure 34. Measured and modeled maximum frequency of oscillation, f_{MAX}, as a function of temperature.

2.7 Conclusion

Extensive dc and RF characterization has been performed for evaluation of device performance and extraction of bias-dependent model elements for use in a large signal model. Pulse testing and elevated temperature measurements have been performed, showing how thermal effects can be quantified and isolated from other gain-degrading effects. This leads to an accurate understanding of the HBT at high power densities hence accurate modeling of the many interdependent effects.

Also for use in high power applications, a true large signal nonlinear model has been developed which incorporates the effects of saturation, cutoff, the Kirk effect, and the thermal effects. The model has been implemented in a harmonic balance simulator with excellent agreement to on-wafer power and harmonic measurements as well as dc and pulsed measurements. The model also gives access to RF current an voltage waveforms as well as low frequency temperature waveforms which were beyond the capabilities of laboratory experiments. By knowing such information, many mechanisms can be understood such as the cause of output saturation and the behavior of harmonics.

An analysis of the most temperature-sensitive microwave elements for the HBT has been performed. These equivalent circuit elements, R_{eb}, C_{eb}, and g_m, showed consistent change with temperature and agreed well in magnitude and direction with a rigorous physical model evaluated from 23°C to 226°C. In the absence of saturation effects caused by the parasitic R_b and R_e, R_{eb} was found to decrease by an average of 1.3% per°C at constant V_{be}. Similarly, g_m was found to increase by an average of 1.4% per°C and C_{eb} by 0.8% per°C. These changes are shown to be consistent with a decrease in current gain at constant I_b. Effects observed from the raw data included a drop in frequency response with temperature, specifically f_T decreased by approximately 0.2% per°C and f_{MAX} decreased by 0.3% per°C. The measured and modeled behavior of the microwave element values and cutoff frequencies is useful for developing a temperature-dependent large signal microwave model which has its basis on device physics. The employed one-dimensional physical HBT modeling has been shown to give an accurate indication of the relative changes in important microwave equivalent circuit elements with temperature and bias.

2.8 Future Work

From the bias- and temperature-dependent microwave characterization and modeling, a new microwave large signal temperature-dependent model can be developed. This model would be based on true *microwave* temperature effects as opposed to only dc and pulsed. Microwave large signal elements will dynamically follow the locus of small signal elements versus bias for a particular temperature. In addition, the actual and theoretical change in this locus with temperature has been presented and can be added to the large signal dependencies.

Since the currently existing large signal model is based on room temperature microwave measurements, and on dc and pulsed thermal effects, it can be used effectively to develop biasing topologies which reduce the dependence of circuit performance on temperature. for instance, if an HBT is biased with constant V_{be} instead of constant I_b, the base I-V temperature effects partially compensate for the gain reduction effect on collector current. A strictly constant V_{be} bias, however, can lead to thermal runaway through the exponential increase of I_b with temperature. Based on the developed models of these effects, circuit topologies which are adaptive in nature can maintain constant dc and microwave performance over a range of bias and input power levels.

2.9 Acknowledgements

The authors wish to thank the Ar Force Wright Laboratory, particularly G.J. Trombley, M.E. Cheney, and C.J. Huang, for supplying devices and helpful discussions.

3. Publications

D.S. Whitefield, C.J. Wei, J.C.M. Hwang, "High Power Characterization and Modeling of Heterojunction Bipolar Transistors," 1992 IEEE Princeton Section Sarnoff Symposium Digest, Session II.

D.S. Whitefield, C.J. Wei, J.C.M. Hwang, "Temperature Dependent Large Signal Model of Heterojunction Bipolar Transistors," 1992 GaAs IC Symposium, pp. 221-224.

C.J. Wei, B.R.A. Sugeng, J.C.M. Hwang, "A Microwave SPICE Model for Double-Heterojunction Bipolar Transistors," 1993 IEEE Princeton Section Sarnoff Symposium Digest, Session IIb.

Manuscripts in preparation for submission:

D.S. Whitefield, C.J. Wei, J.C.M. Hwang, "An Analysis of Thermal Effects on the Microwave Performance of Heterojunction Bipolar Transistors," Submitted to IEEE Transactions on Electron Devices.

D.S. Whitefield, C.J. Wei, J.C.M. Hwang, "Microwave Thermal Effects of the Heterojunction Bipolar Transistor," To be submitted to the 1993 GaAs IC Symposium.

4. Professional Personnel

Dr. J.C.M. Hwang
Professor of Electrical Engineering and
Director of Compound Semiconductor Technology Laboratory, Lehigh University.

Dr. C.J. Wei
Research Scientist, Compound Semiconductor Technology Laboratory, Lehigh University.

D.S. Whitefield
Graduate Student and Research Assistant.
M.S., Electrical Engineering, Lehigh University, 1991. Thesis: Large Signal Characterization and Modeling of Heterojunction Bipolar Transistors.
Ph.D., Electrical Engineering, Lehigh University, 1993. Dissertaion: Thermal Characterization and Modeling of Heterojunction Bipolar Transistors.

5. Presentations

- Location: Wright Laboratory, Wright Patterson AFB, Ohio. December, 1991.
  Speaker: D.S. Whitefield
  Title: HBT Thermal Effects.

- Location: Wright Laboratory, Wright Patterson AFB, Ohio. December 1991.
  Speaker: C.J. Wei
  Title: Large Signal Modeling of the Heterojunction Bipolar Transistor.

- Location: David Sarnoff Research Center, Princeton NJ. March, 1992.
  Speaker: D.S. Whitefield
  Title: High Power Characterization and Modeling of Heterojunction Bipolar Transistors.

- Location: NEC Corporation, Tsukuba, Japan, July 1992.
  Speaker: D.S. Whitefield
  Title: Temperature Dependent Large Signal Model of Heterojunction Bipolar Transistors.

- Location: NTT Corporation, Atsugi, Japan, August 1992.
  Speaker: D.S. Whitefield
  Title: Temperature Dependent Large Signal Model of Heterojunction Bipolar Transistors.

- Location: Fujitsu Corporation, Atsugi, Japan, August 1992.
  Speaker: D.S. Whitefield
  Title: Temperature Dependent Large Signal Model of Heterojunction Bipolar Transistors.

- Location: IEEE GaAs IC Symposium, Miami Beach, FL, October 1992.
  Speaker: J.C.M. Hwang
  Title: Temperature Dependent Large Signal Model of Heterojunction Bipolar Transistors.

- Location: Lehigh University, Bethlehem, PA, November 1992.
  Speaker: D.S. Whitefield
  Title: Bipolar Transistor Thermal Effects.

- Location: David Sarnoff Research Center, Princeton NJ. March, 1993.
  Speaker: C.J. Wei
  Title: A Microwave SPICE Model for Double-Heterojunction Bipolar Transistors.

6. Interactions

Dr. Hwang is a consultant to the Air Force Wright Laboratory in the areas of MMIC processing and material/device correlation. Dr. Hwang spends 20% of his time at Wright Laboratory and both written and oral progress reports on HBTs are provided regularly to Dr. Chern Huang and his colleagues. The HBT devices used for this work were fabricated at Wright Laboratory using their in-house MBE process.

D.S. Whitefield is a Second Lieutenant in the Air Force Reserves, currently on a four year educational delay to complete his Ph.D. degree in Electrical Engineering. In July 1990 and December 1991, D.S. Whitefield spent one week at the Ar Force Wright Laboratory discussing microwave device fabrication, characterization, and modeling. D.S. Whitefield will begin reserve duty upon graduation.

Dr. Wei also spent one week in December 1991 at the Air Force Wright Laboratory discussing microwave device fabrication, characterization, and modeling.

7. Inventions

There have been no inventions for this report period (DD Form 882 Attached).

REPORT OF INVENTIONS AND SUBCONTRACTS

(Pursuant to "Patent Rights" Contract Clause) (See Instructions on Reverse Side.)

Form Approved
OMB No. 0704-0237
Expires Jun 30, 1992

1a. NAME OF CONTRACTOR/SUBCONTRACTOR	c. CONTRACT NUMBER	2a. NAME OF GOVERNMENT PRIME CONTRACTOR	c. CONTRACT NUMBER	3. TYPE OF REPORT (X one)
Lehigh University	AFOSR-90-0302	Same	Same	a. INTERIM [ ] b. FINAL [X]
b. ADDRESS (Include ZIP Code)	d. AWARD DATE (YYMMDD)	b. ADDRESS (Include ZIP Code)	d. AWARD DATE (YYMMDD)	4. REPORTING PERIOD (YYMMDD)
Packard Lab. #19 Bethlehem, PA 18015	900601	Same	Same	a. FROM 900601 b. TO 930531

SECTION I – SUBJECT INVENTIONS

5. "SUBJECT INVENTIONS" REQUIRED TO BE REPORTED BY CONTRACTOR/SUBCONTRACTOR (If "None," so state)

a. NAME(S) OF INVENTOR(S) (Last, First, MI)	b. TITLE OF INVENTION(S)	c. DISCLOSURE NO., PATENT APPLICATION SERIAL NO. OR PATENT NO.	d. ELECTION TO FILE PATENT APPLICATIONS				e. CONFIRMATORY INSTRUMENT OR ASSIGNMENT FORWARDED TO CONTRACTING OFFICER	
			(1) United States		(2) Foreign			
			(a) Yes	(b) No	(a) Yes	(b) No	(1) Yes	(2) No
None								

f. EMPLOYEE OF INVENTOR(S) NOT EMPLOYED BY CONTRACTOR/SUBCONTRACTOR		g. ELECTED FOREIGN COUNTRIES IN WHICH A PATENT APPLICATION WILL BE FILED	
(1) (a) Name of Inventor (Last, First, MI)	(2) (a) Name of Inventor (Last, First, MI)	(1) Title of Invention	(2) Foreign Countries of Patent Application
(b) Name of Employer	(b) Name of Employer		
(c) Address of Employer (Include ZIP Code)	(c) Address of Employer (Include ZIP Code)		

SECTION II – SUBCONTRACTS (Containing a "Patent Rights" clause)

6. SUBCONTRACTS AWARDED BY CONTRACTOR/SUBCONTRACTOR (If "None," so state)

a. NAME OF SUBCONTRACTOR(S)	b. ADDRESS (Include ZIP Code)	c. SUBCONTRACT NO.(S)	d. DFAR "PATENT RIGHTS"		e. DESCRIPTION OF WORK TO BE PERFORMED UNDER SUBCONTRACT(S)	f. SUBCONTRACT DATES (YYMMDD)	
			(1) Clause Number	(2) Date (YYMM)		(1) Award	(2) Estimated Completion
None							

SECTION III – CERTIFICATION

7. CERTIFICATION OF REPORT BY CONTRACTOR/SUBCONTRACTOR (Not required if [ ] Small Business or [ ] Non-Profit organization) (X appropriate box)

a. NAME OF AUTHORIZED CONTRACTOR/SUBCONTRACTOR OFFICIAL (Last, First, MI)	c. I certify that the reporting party has procedures for prompt identification and timely disclosure of "Subject Inventions," that such procedures have been followed and that all "Subject Inventions" have been reported.	
John M. Cheezum Jr.		
b. TITLE	d. SIGNATURE	e. DATE SIGNED
Director, Office of Research and Sponsored Programs	John M. Cheezum Jr.	6/7/93